Sensing and Bio-Sensing Research 12 (2017) 8–14

Contents lists available at ScienceDirect

Sensing and Bio-Sensing Research

journal homepage: www.elsevier.com/locate/sbsr

A new structure of photonic crystal fiber with high sensitivity, high nonlinearity, high birefringence and low confinement loss for liquid analyte sensing applications

Md. Faizul Huq Arif *, Md. Jaminul Haque Biddut

Department of Information and Communication Technology, Mawlana Bhashani Science and Technology University, Santosh, Tangail-1902, Bangladesh

ARTICLE INFO

Article history:
Received 27 July 2016
Received in revised form 4 November 2016
Accepted 8 November 2016

Keywords:
Liquid sensor
Fiber optics sensor
Photonic crystal fiber
Rotated hexagonal cladding
Nonlinear optics

ABSTRACT

This paper proposes the design and optimization of microstructure optical fiber for liquid sensing applications. A number of propagation characteristics have been compared between two formations of hexagonal cladding of our proposed PCF structure. The core of the proposed PCF structure is designed with two rows of supplementary elliptical air holes. We investigate the performance of the designed PCFs for Ethanol as a liquid sample to be sensed. Numerical analysis is carried out by employing the full vectorial Finite Element Method (FEM) to examine the modal birefringence, confinement loss, relative sensitivity and nonlinear coefficient of the proposed PCF structure.

1. Introduction

Photonic Crystal Fiber (PCF) is a new class of optical waveguides has received a tremendous attention since the last decade [1]. PCF offers remarkable characteristics such as design flexibility, geometric versatility and exceptional guiding mechanism which tend to better performance compared to conventional optical fiber [2]. Due to having the well-known optical guiding properties such as high birefringence, low confinement loss, high nonlinearity, the endlessly single mode, flexible chromatic dispersion, large effective mode area and a small bending loss PCFs show a great potentiality in developing different optical functional devices [3–10]. However, in recent years, PCFs have been attracted a great deal of attention to the researchers for sensing applications [11].

Conventional optical sensors are commercially available [12], while PCF based sensors are still in development stage [11]. However, researchers are working for interfacing PCF based sensors in industrial safety purposes and environmental monitoring issues. PCF technology allows us to achieve exceptional propagation properties of fiber through changing the air hole shape, size and their position [13]. Various research studies of PCF based sensors have been reported to improve the performance of PCF with better propagation properties by changing different geometric parameters. Hollow-core Photonic Band Gap (PBG) PCFs are convenient for gas sensing applications. In contrast, for the liquid sensing applications, index guided PCFs are suitable. The sensing mechanism of index guided PCF is based on the evanescent interaction between guided electro-magnetic light mode and a sample (liquids or gasses), similar to that in traditional optical fiber sensors [12]. Recently, the concept of filling the PCF holes with different materials (gasses and liquids) opened a route for chemical and biological sensing [14,15]. There are several number of published papers which have investigated and developed the evanescent field sensing approach of PCF. Monro et al. [16] have introduced a PCF structure for evanescent field sensing whereby both core and cladding are microstructured. Cordeiro et al. [17] have demonstrated that the PCF structure in which both core and cladding are microstructured helps to increase electromagnetic power interaction with the sample to be sensed. Using this type of structure, the authors have stated in the articles [18–25] that their proposed PCF structures show higher relative sensitivity with low confinement loss for liquid and gas sensing applications. The authors in [3] have demonstrated that their proposed PCF structure for liquid sensor is simple and cost effective.

In some especial fiber optic sensors maintaining the state of polarization in fiber is crucial. Traditional Single Mode Fibers (SMFs) cannot maintain the polarization state of the electromagnetic field for many reasons, as stated in [26]. However, the polarization condition can be retained through the application of modal birefringence. High birefringent PCFs are highly intensive to temperature, which is an important feature for different sensing applications [11]. The articles [27–29] show that elliptical holes are responsible to achieve birefringence in PCF. The authors of the articles [28,29] demonstrated that their designed PCFs can achieve the birefringence up to the order of 10^{-2}. However, these PCFs show poor light confinement and high propagation loss. To

* Corresponding author.
E-mail address: arifict27@gmail.com (M.F.H. Arif).

http://dx.doi.org/10.1016/j.sbsr.2016.11.003

overcome the limitations of poor mode of confinement, the article [31] proposed a PCF structure for liquid sensing applications which show good confinement of light. In the research article [30] authors have proposed a nonlinear PCF structure for gas sensing applications which shows high sensitivity with high birefringence, but the nonlinearity of the PCF is comparatively low.

In this study, we have proposed a PCF structure for liquid sensing applications in which both core and cladding are microstructured. The core holes are infiltrated with the targeted liquid. Generally, water or alcohol is treated as primary liquids; the numerical analysis has been done for Ethanol detection. In this PCF cladding air holes are circular and the supplementary core holes are elliptical.

2. Design Principle

In this work, we have proposed and analyzed an index guided PCF structure with hexagonal arrangement of air holes in cladding. From the Fig. 1(a) and (b), we can easily understand the difference between conventional hexagonal cladding and 90^0 rotated hexagonal cladding respectively. In both proposed structures the diameter of each air hole in the cladding is $d = 1.9$ μm. The number of air hole rings in the cladding is set to $N = 4$. One of the special features of the proposed PCF structures is that the core region is designed with vertically arranged supplementary elliptical air holes, which is filled with the targeted sample (Ethanol). The enlarged cross sectional view of the core region is shown in Fig. 1(c). Size of each elliptical air hole on the lattice is $A = 0.47$ μm^2 and theif ellipticity constant, $\eta = a/b = 0.6$, where, a and b are half minor axis and half major axis respectively. This arrangement of core results in higher birefringence. In this simulation, the center-to-center spacing (pitch) between two air holes in the cladding is set to $\Lambda = 2.4$ μm. In the core, two different pitches have been taken to design, where, $\Lambda_a = 0.65$ μm and $\Lambda_b = 1.20$ μm are horizontal pitch and vertical pitch respectively. The background material is pure silica and in the calculations, the refractive index of silica is determined by the following Sellmeier equation [32].

$$n(\lambda) = \sqrt{1 + \frac{B_1\lambda^2}{\lambda^2 - C_1} + \frac{B_2\lambda^2}{\lambda^2 - C_2} + \frac{B_3\lambda^2}{\lambda^2 - C_3}} \tag{1}$$

where, n is the refractive index of silica, λ is the operating wavelength in μm, $B_{(i=1,\ 2,\ 3)}$ and $C_{(i=1,\ 2,\ 3)}$ are Sellmeier coefficients. Perfectly Matched Layer (PML) is used as a boundary condition and the thickness of PML is set to 10% of the radius of the proposed PCF for effective calculation of confinement loss [6].

3. Simulation and principle of operations

In this study, the full vectorial Finite Element Method (FEM) with Perfectly Matched Layer (PML) boundary condition is adopted for the analysis of the structure with a FEM based simulation software COMSOL Multiphysics 4.2. The modal analyses have been performed on the cross section in the x-y plane of the PCF structure as the wave is propagating in the z direction. The radiation through the proposed PCF is guided by the modified total internal reflection. The following equation with a magnetic field formulation can be derived from the Maxwell equations [33].

$$\nabla \times \left(\varepsilon_r^{-1} \nabla \times \vec{H}\right) - K_0^2 \mu_r \vec{H} = 0 \tag{2}$$

where, $\vec{H}$ is the magnetic field, ε_r and μ_r are the relative dielectric permittivity and magnetic permeability respectively. The symbol K_0 is the wave number in vacuum; where $K_0 = 2\pi/\lambda$, λ is the operating wavelength. The magnetic field of the modal solution can be expressed as $\vec{H} = \vec{h}(x,y)\exp(-j\beta z)$; where, $\vec{h}(x,y)$ is the field distribution on the transverse plane. The propagation constant β is represented as $\beta = n_{eff}K_0$. After obtaining the complex modal effective index (n_{eff}), the modal birefringence can be determined by the following equation.

$$B \equiv \left| n_{eff}^x - n_{eff}^y \right| \tag{3}$$

where, n_{eff}^x and n_{eff}^y are the effective refractive indices of the x and y polarized fundamental mode respectively. The finite air holes in the cladding part cause the leakage of light from core to exterior part which results in confinement losses. The confinement loss can be calculated from the imaginary part of the complex effective index n_{eff}^i, using the following equation [1].

$$L_c = \frac{40\pi.\mathrm{Im}\left[n_{eff}^i\right] \times 10^6}{\lambda.\ln(10)}\mathrm{dB/m}(i = x,y) \tag{4}$$

However, by using an infinite number of air holes the leakage of light can be omitted. But in practical the number of air holes is finite. The evanescent field interaction between light and the targeted sample can be measured by the relative sensitivity coefficient. According to the Beer-Lambert law, light is attenuated by the intensity of the evanescent wave absorption [34].

$$I(\lambda) = I_0(\lambda)\exp[-r\alpha_m lc] \tag{5}$$

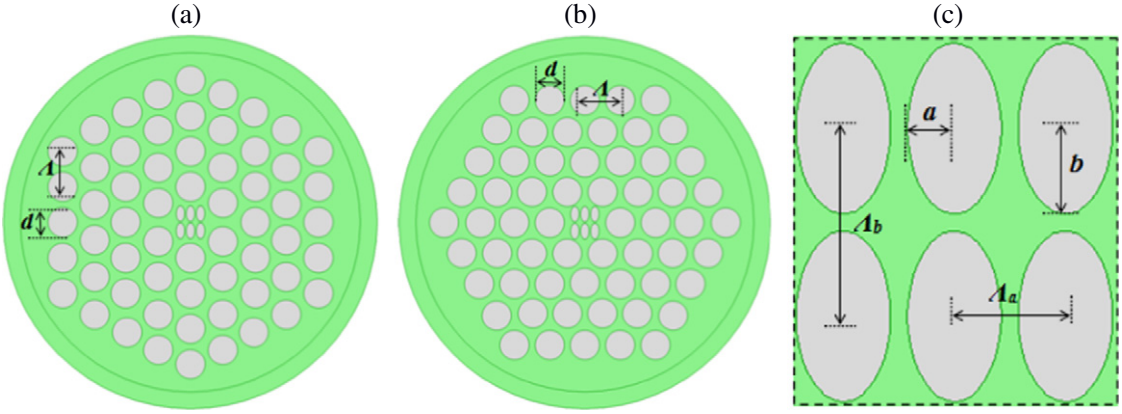

Fig. 1. Cross section of the proposed designs: (a) PCF_1: conventional hexagonal cladding (b) PCF_2: rotated hexagonal cladding (c) enlarged view of the core region.

The absorption of the targeted sample can be defined by the following equation [3,18].

$$A = \log\left(\frac{I}{I_0}\right) = r\alpha_m lc \tag{6}$$

where I and I_0 are the input and output intensities accordingly. The symbol l represents the length of the fiber and c is the concentration of the sample. The absorption coefficient is α_m and r is the relative sensitivity coefficient which is expressed by the following equation [17].

$$r = \frac{n_r}{\mathrm{Re}[n_{eff}]} f \tag{7}$$

where n_r refers to the refractive index of the targeted sample and Re[n_{eff}] is the real part of effective refractive index and f is the fraction of total power located in the core. According to the Poynting's theorem f can be expressed as [17]

$$f = \frac{\int_{sample} \mathrm{Re}(E_x H_y - E_y H_x)\,dxdy}{\int_{total} \mathrm{Re}(E_x H_y - E_y H_x)\,dxdy} \tag{8}$$

where, the transverse electric and magnetic fields of the modes are introduced by E_x, E_y and H_x, H_y respectively. These transverse fields and effective index mode n_{eff} can be calculated by solving Maxwell equation.

Effective mode area is also an important parameter to determine the optical performance of PCF. The effective area of a PCF can be determined by the following equation [35].

$$A_{eff} = \frac{\left(\int\int |E|^2 dxdy\right)^2}{\int\int |E|^4 dxdy} \tag{9}$$

The nonlinear coefficient γ is given by the following formula [36].

$$\gamma = \frac{2\pi \cdot \mathrm{n}_2}{\lambda \cdot A_{eff}} \tag{10}$$

where n_2 is the nonlinear refractive index of the fiber. According to the equation, it is clear that the nonlinear coefficient of a PCF is inversely related to the effective area.

4. Numerical results and discussions

The numerical analyses on some propagation characteristics of the proposed PCF structures in fundamental mode and some higher order modes have been discussed in this section. Ethanol has been selected for filling the supplementary core holes. The simulation has been performed effectively at a wide range of wavelength from 0.8 μm to 1.8 μm. Initially, characteristics of the effective refractive index of the proposed structures have been studied. The numerical investigation in Fig. 2(a) shows the effective index profiles of the proposed PCF structures at different wavelengths. For both formation of the proposed PCF structure, an increase in the operating wavelength results in a linear decrease in effective indices. Fig. 2(b) illustrates that the effective refractive index values of both designed structures are decreasing by the increase of the ellipticity constant of the supplementary core holes, where the operating wavelength is fixed to 1.3 μm.

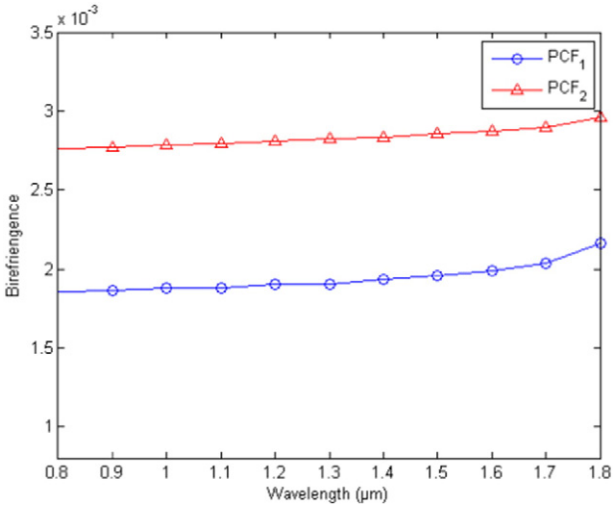

Fig. 3. Variation of the modal birefringence for PCF_1 and PCF_2 as a function of wavelength, where $\eta = a/b = 0.6$.

Fig. 3 depicts the wavelength dependent modal birefringence, where $\eta = 0.6$. It can be evidently seen that the proposed PCF2 structure shows higher birefringence than the proposed PCF1 structure. In addition, it is clear from the Fig. 3 that the birefringence values are gradually increasing with the operating wavelength.

The Fig. 4(a)–(c) illustrate the resultant 2D views of mode field profiles in x- and y-Polarized modes with the variation of the ellipticity constant η, where the operating wavelength is set to 1.3 μm. It can be observed that the fundamental mode is more strongly bonded in the core region of PCF_2 than the PCF_1. Therefore, there is a significant affect of the formation of cladding air holes on field profiles. It can also be seen from the Fig. 4 that for the both proposed structures, the birefringence is decreasing when the ellipticity constant η is increasing. Our calculations show that the modal birefringence values of the proposed PCF_1 and PCF_2

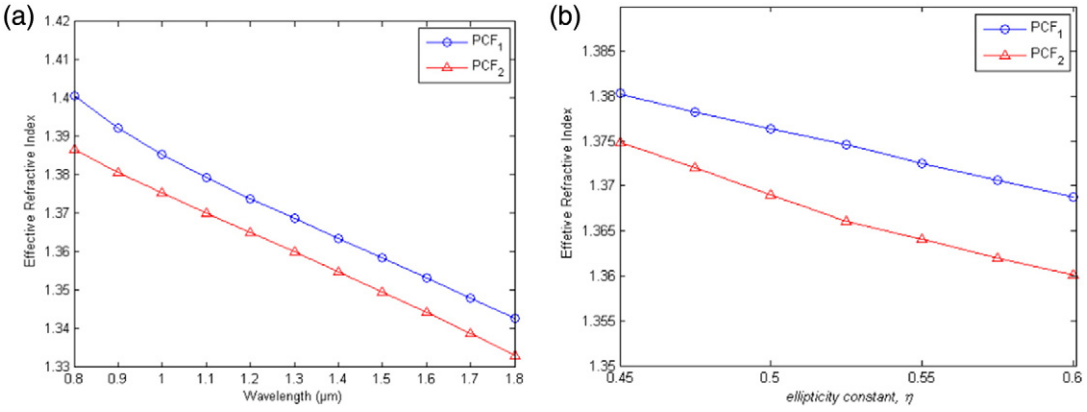

Fig. 2. The effective refractive index of the fundamental mode (a) as a function of wavelength, where $\eta = a/b = 0.6$ and (b) as a function of the ellipticity constant η, where the wavelength is set to $\lambda = 1.3$ μm.

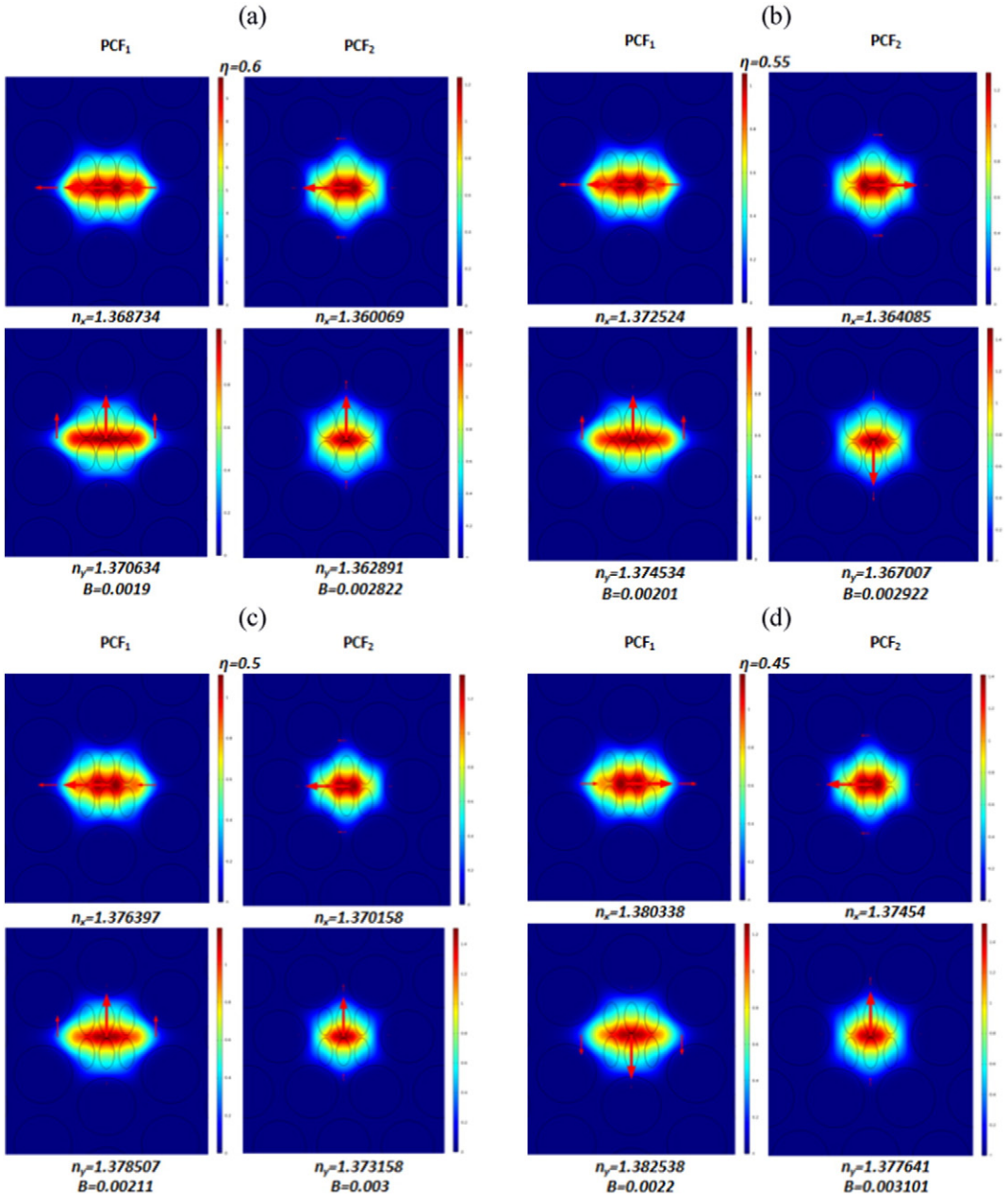

Fig. 4. The field profiles of the proposed PCF structures in x- and y-polarized modes with the ellipticity constant η at the wavelength $\lambda = 1.3$ μm. (a) $\eta = a/b = 0.6$, (b) $\eta = a/b = 0.55$, (c) $\eta = a/b = 0.50$ and (d) $\eta = a/b = 0.45$.

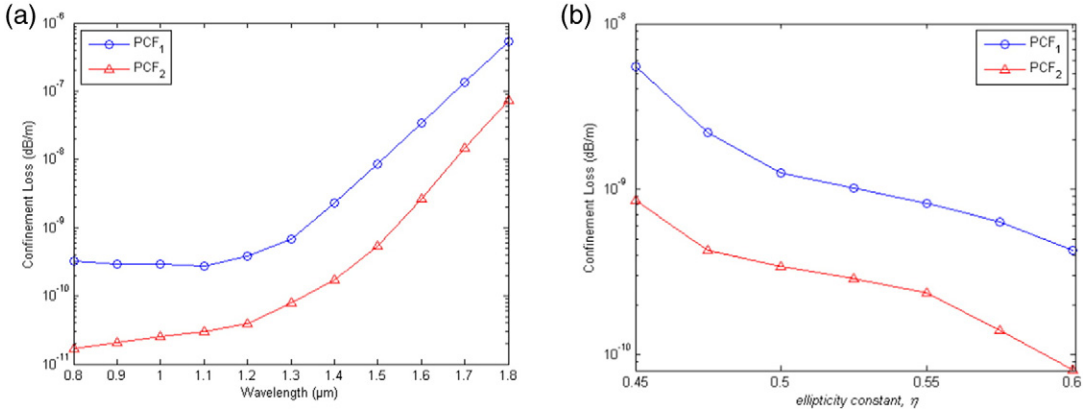

Fig. 5. (a) Confinement loss versus wavelength for the proposed PCF structures, where $\eta = 0.6$ and (b) variation of confinement loss as a function of the ellipticity constant η, where the operating wavelength λ is fixed to 1.3 μm.

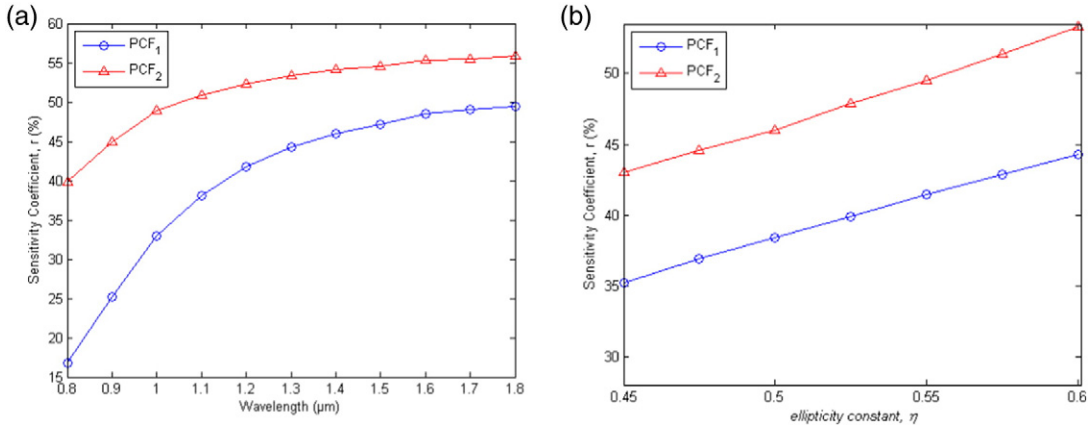

Fig. 6. (a) Relative sensitivity versus wavelength for the proposed PCF structures, where $\eta = 0.6$ and (b) variation of relative sensitivity as a function of the ellipticity constant η, where the operating wavelength λ is fixed to1.3 μm.

are 1.90×10^{-3} and 2.822×10^{-3} respectively at the wavelength $\lambda = 1.3$ μm with the optimized design parameters. This result indicates that rotated hexagonal cladding improves the birefringence of the proposed structure. Moreover, the birefringence of the proposed PCF_2 is higher than the acquired birefringence in a recently published research article for liquid sensing application [31].

The measurement of mode confinement of the guided light is one of the key parameters of PCF based devices. The electromagnetic radiation propagates through the proposed PCF structures. However, a small portion of the incident energy is leaking out of the core. Hence, the confinement losses of the proposed PCFs need to be measured to evaluate their performance. Fig. 5(a) presents the confinement loss curves of the proposed PCF structures as a function of the operating wavelength. On the other hand, Fig. 5(b) depicts the effect of the ellipticity constant η on the confinement losses of both the proposed PCF structures. Moreover, with an inquiry of Fig. 5(b), it is clear that the confinement losses decrease with an increase of the ellipticity constant value of the core holes. The confinement losses of the PCF_1 and PCF_2 are 2.87×10^{-10} dB/m and 1.62×10^{-10} dB/m respectively, when $\lambda = 1.3$ μm and $\eta = 0.6$. In case of Ethanol as the supplementary core material, the calculated confinement losses for both the proposed PCFs are lower than the previously published articles [1,3,11,31].

The relative sensitivity coefficient is one of the most vital parameters for PCF based sensing devices. As presented before in Fig. 5 that the fundamental mode of the proposed PCF having rotated hexagonal cladding is more confined than the proposed PCF having conventional hexagonal cladding. Hence, the interaction between light and the analyte (Ethanol) in the core region of the proposed PCF_2 structure is expected to be higher than the proposed PCF_1 structure. Fig. 6(a) shows the wavelength dependent relative sensitivity coefficient r for Ethanol detection, where $\eta = 0.6$ is fixed. It is evidently seen from the Fig. 6(a) that the relative sensitivity coefficient is increasing according to the operating wavelength. Moreover, Fig. 6(b) represents the relationship between relative sensitivity and the ellipticity constant of the core holes of the proposed PCF structures. Furthermore, it can be clearly seen that the relative sensitivity is increasing when the ellipticity constant values are increasing. In addition, at the wavelength $\lambda = 1.3$ μm and $\eta = 0.6$, the relative sensitivity coefficient values of the proposed PCF_1 and PCF_2 are 44.29% and 53.35% accordingly. Therefore, it is clear that rotated hexagonal cladding of the proposed PCF improves sensitivity approximately 20%. In addition, the proposed PCF_2 shows higher sensitivity than the acquired sensitivity in the previously proposed PCF structures in case of liquid sensing applications [1,3,11,31].

Fig. 7 represents the effective mode area values of the proposed PCF_1 and PCF_2 by varying the operating wavelength. It shows that the effective mode area A_{eff} increases with the wavelength. The reason behind that, when the wavelength increases the modes are leaking through the air holes. However, it can also be seen from the Fig. 7 that PCF_1 shows larger effective area than PCF_2. It can be seen that at the wavelength $\lambda = 1.3$ μm and the ellipticity constant $\eta = 0.6$, the effective mode area values of the proposed PCF_1 and PCF_2 are 7.5782μm^2 and 3.9328μm^2 respectively.

Fig. 8 shows the wavelength dependent nonlinear coefficient for the proposed PCF structures. It illustrates that the nonlinear coefficient γ decreases with the increase of wavelength. Small effective mode area tends to a high nonlinear coefficient that might be useful in various optical applications. It can be clearly seen from Fig. 4 that the proposed PCF_2 exhibits smaller effective mode area than the proposed PCF_1.

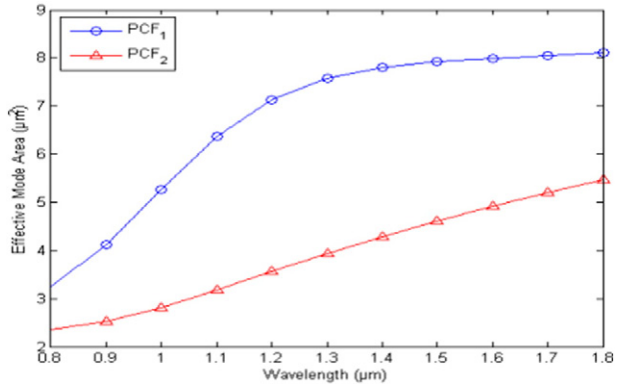

Fig. 7. Variation of effective mode area with the operating wavelength for the proposed PCFs, $\eta = 0.6$.

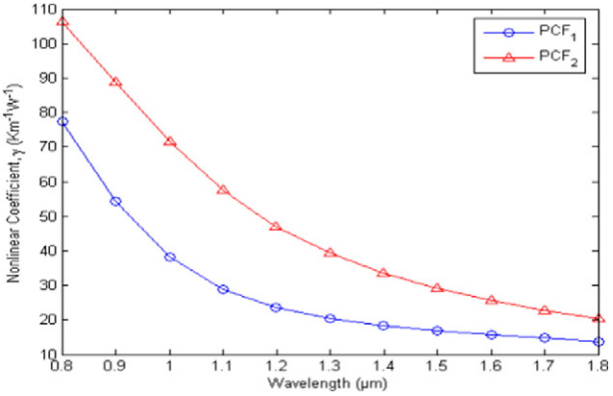

Fig. 8. Variation of nonlinear coefficients with the operating wavelength for the proposed PCFs, $\eta = 0.6$.

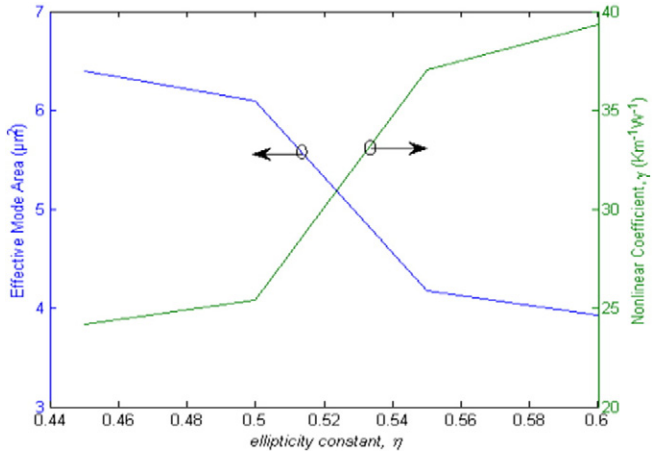

Fig. 9. Variation of effective mode area and nonlinear coefficients with the ellipticity constant η for the proposed PCF_2 at the operating wavelength $\lambda = 1.3$ μm.

Therefore, in Fig. 8, PCF_2 shows higher nonlinearity than PCF_1. Simulation results show that the nonlinear coefficients of the proposed PCF_1 and PCF_2 in the x-polarized mode are reported as 20.41 W^{-1} km^{-1} and 39.33 W^{-1} km^{-1} respectively at the wavelength $\lambda = 1.3$ μm. For the calculation of the nonlinearity index of silica is taken as $n_2 = 3.2 \times 10^{-20}$ m^2/W.

Fig. 9 describes the ellipticity constant dependence of effective mode area and nonlinear coefficient of the proposed PCF_2 at the operating wavelength 1.3 μm. It is observed that effective mode area decreases with an increase in ellipticity constant and vice-versa for nonlinear coefficient.

We have also observed from the simulation that there are no significant changes in the birefringence, confinement loss, relative sensitivity and the nonlinear coefficients of the fundamental modes by varying the number of air hole rings at the cladding from 3 to 6. Therefore, from the consideration of fabrication cost, we have selected 4 rings of air holes for the optimization of our proposed PCF structure. Our proposed PCF structure can be fabricated by presently available technology due to the advancement of nanotechnology. Several methods have been developed for the fabrication of microstructured fiber efficiently, such as stack and draw [37], drilling [38], extrusion [39], sol-gel casting [40] and so on. However, micro core of our designed PCF must be filled with analyte without damaging the fiber's integrity. Authors of the article [41] proposed a technique for selectively filling the micro holes. In addition, recently, Luo et al. [42] and Gerosa et al. [43] have practically shown that using the similar methods the fabrication of PCF structures with liquid filled core or cladding holes can be accomplished efficiently. Therefore, we believe that our proposed PCF structure can be interfaced with existing technologies.

According to the above discussion, to gain high performance of PCF based sensor, the optimized parameters of the proposed PCF structure are found as $\Lambda = 2.4$ μm, $d = 1.9$ μm, $N = 4$ and $\eta = 0.6$ μm. Our proposed PCF structure is demonstrated to gain a good tolerance of fabrication errors. However, in a standard fiber draw, $\pm 1\%$ variations in fiber global diameter may occur during the fabrication process [44]. To account for this structural variation, the global parameters have been varied up to $\pm 5\%$ around the designed values to reveal the robustness of the proposed design. Table 1 represents the values of the above properties of the proposed PCF_2 for the changes in global parameters.

Table 1
Variation of different index guiding properties of the proposed PCF_2 for the changes in global parameters at the wavelength $\lambda = 1.3$ μm.

Parameters (%)	B	L_c (dB/m)	R (%)	γ (W^{-1} km^{-1})
−5	2.87×10^{-3}	1.07×10^{-9}	47.76	38.559
Optimum	2.82×10^{-3}	1.62×10^{-10}	53.35	39.330
+5	2.71×10^{-3}	8.74×10^{-11}	58.79	39.807

5. Conclusion

To summarize, we have successfully demonstrated high sensitivity, high nonlinearity, high birefringence and low confinement loss with our proposed PCF structures. The effects of 90° rotation of hexagonal cladding on different guiding properties have been studied. In addition, it was found that there is a significant effect of the ellipticity constant of supplementary core holes on the overall performance of the proposed structure. The numerical inquiry shows that the proposed hexa-rotated cladding structure (PCF_2) exhibits comparatively higher relative sensitivity, nonlinearity, and birefringence. The figures are 53.35%, 39.330 W^{-1} km^{-1}, and 2.82×10^{-3} respectively. Apart from that, the confinement loss of this structure is very low; the value is 1.62×10^{-10} dB/m.

According to the performance analysis, we expect that the proposed structure will open a new window in the field of PCF based sensing. In addition, having greater ability to perform liquid analyte sensing, the proposed PCF structure may be optimal for different bio-sensing applications.

References

[1] H. Ademgil, Highly sensitive octagonal photonic crystal fiber based sensor, Opt. Int. J. Light Electron Opt. 125 (20) (2014) 6274–6278.
[2] A.M. Pinto, M. Lopez-Amo, Photonic crystal fibers for sensing applications, J. Sens. 2012 (2012).
[3] M.F.H. Arif, K. Ahmed, S. Asaduzzaman, M.A.K. Azad, Design and optimization of photonic crystal fiber for liquid sensing applications, Photon. Sens. (2016) 1–10.
[4] T.A. Birks, J.C. Knight, P.S.J. Russell, Endlessly single-mode photonic crystal fiber, Opt. Lett. 22 (13) (1997) 961–963.
[5] A. Ortigosa-Blanch, J.C. Knight, W.J. Wadsworth, J. Arriaga, B.J. Mangan, T.A. Birks, P.S.J. Russell, Highly birefringent photonic crystal fibers, Opt. Lett. 25 (18) (2000) 1325–1327.
[6] M. Morshed, M.I. Hasan, S.A. Razzak, Enhancement of the sensitivity of gas sensor based on microstructure optical fiber, Photon. Sens. 5 (4) (2015) 312–320.
[7] A.M. Cubillas, S. Unterkofler, T.G. Euser, B.J. Etzold, A.C. Jones, P.J. Sadler, P. Wasserscheid, P.S.J. Russell, Photonic crystal fibres for chemical sensing and photochemistry, Chem. Soc. Rev. 42 (22) (2013) 8629–8648.
[8] T. Yang, E. Wang, H. Jiang, Z. Hu, K. Xie, High birefringence photonic crystal fiber with high nonlinearity and low confinement loss, Opt. Express 23 (7) (2015) 8329–8337.
[9] J. Limpert, T. Schreiber, S. Nolte, H. Zellmer, A. Tünnermann, R. Iliew, F. Lederer, J. Broeng, G. Vienne, A. Petersson, et al., High-power air-clad large-mode-area photonic crystal fiber laser, Opt. Express 11 (7) (2003) 818–823.
[10] M. Vieweg, T. Gissibl, S. Pricking, B.T. Kuhlmey, D.C. Wu, B.J. Eggleton, H. Giessen, Ultrafast nonlinear optofluidics in selectively liquid-filled photonic crystal fibers, Opt. Express 18 (24) (2010) 25232–25240.
[11] H. Ademgil, S. Haxha, Highly birefringent nonlinear PCF for optical sensing of analytes in aqueous solutions, Opt. Int. J. Light Electron Opt. 127 (16) (2016) 6653–6660.
[12] H.W. Lee, M.A. Schmidt, P. Uebel, H. Tyagi, N.Y. Joly, M. Scharrer, P.S.J. Russell, Optofluidic refractive-index sensor in step-index fiber with parallel hollow microchannel, Opt. Express 19 (9) (2011) 8200–8207.
[13] K. Ahmed, M. Morshed, Design and numerical analysis of microstructured-core octagonal photonic crystal fiber for sensing applications, Sens. BioSens. Res. 7 (2016) 1–6.
[14] J.B. Jensen, P.E. Hoiby, G. Emiliyanov, O. Bang, L.H. Pedersen, A. Bjarklev, Selective detection of antibodies in microstructured polymer optical fibers, Opt. Express 13 (15) (2005) 5883–5889.
[15] B.T. Kuhlmey, B.J. Eggleton, D.K. Wu, Fluid-filled solid-core photonic bandgap fibers, J. Lightwave Technol. 27 (11) (2009) 1617–1630.
[16] T.M. Monro, W. Belardi, K. Furusawa, J.C. Baggett, N.G.R. Broderick, D.J. Richardson, Sensing with microstructured optical fibres, Meas. Sci. Technol. 12 (7) (2001) 854.
[17] C.M. Cordeiro, M.A. Franco, G. Chesini, E.C. Barretto, R. Lwin, C.B. Cruz, M.C. Large, Microstructured-core optical fibre for evanescent sensing applications, Opt. Express 14 (26) (2006) 13056–13066.
[18] M.F.H. Arif, S. Asaduzzaman, K. Ahmed, M. Morshed, High sensitive PCF based chemical sensor for ethanol detection, 5th International Conference on Informatics, Electronics and Vision (ICIEV), IEEE, Dhaka, 2016.
[19] M.F.H. Arif, M.J.H. Biddut, K. Ahmed, S. Asaduzzaman, Simulation based analysis of formalin detection through photonic crystal fiber, 5th International Conference on Informatics, Electronics and Vision (ICIEV), IEEE, Dhaka, 2016.
[20] S. Asaduzzaman, M.F.H. Arif, K. Ahmed, P. Dhar, Highly sensitive simple structure circular photonic crystal fiber based chemical sensor, 2015 IEEE International WIE Conference on Electrical and Computer Engineering (WIECON-ECE) 2015, pp. 151–154.

[21] S. Asaduzzaman, K. Ahmed, M.F.H. Arif, M. Morshed, Proposal of a simple structure photonic crystal fiber for lower indexed chemical sensing, 2015 18th International Conference on Computer and Information Technology (ICCIT) 2015, pp. 127–131.
[22] M.F.H. Arif, K. Ahmed, S. Asaduzzaman, A comparative analysis of two different PCF structures for gas sensing application, 2015 International Conference on Advances in Electrical Engineering (ICAEE) 2015, pp. 247–250.
[23] M. Morshed, S. Asaduzzaman, M.F.H. Arif, K. Ahmed, Proposal of simple gas sensor based on micro structure optical fiber, 2015 International Conference on Electrical Engineering and Information Communication Technology (ICEEICT) 2015, pp. 1–5.
[24] M. Morshed, M.I. Hassan, T.K. Roy, M.S. Uddin, S.A. Razzak, Microstructure core photonic crystal fiber for gas sensing applications, Appl. Opt. 54 (29) (2015) 8637–8643.
[25] M. Morshed, M.F.H. Arif, S. Asaduzzaman, K. Ahmed, Design and characterization of photonic crystal fiber for sensing applications, Eur. Sci. J. 11 (12) (2015).
[26] M. Sharma, N. Borogohain, S. Konar, Index guiding photonic crystal fibers with large birefringence and walk-off, J. Lightwave Technol. 31 (21) (2013) 3339–3344.
[27] J. Ju, W. Jin, S. Demokan, Properties of a highly Birefringent Photonic Crystal Fiber, IEEE Photonics Technology Letters, 2003.
[28] S.E. Kim, B.H. Kim, C.G. Lee, S. Lee, K. Oh, C.-S. Kee, Elliptical defected core photonic crystal fiber with high birefringence and negative flattened dispersion, Opt. Express 20 (2) (2012) 1385–1391.
[29] M.J. Steel, R.M. Osgood, Elliptical-hole photonic crystal fibers, Opt. Lett. 26 (4) (2001) 229–231.
[30] S. Asaduzzaman, K. Ahmed, Proposal of a gas sensor with high sensitivity, birefringence and nonlinearity for air pollution monitoring, Sens. BioSens. Res. 10 (2016) 20–26.
[31] H. Ademgil, S. Haxha, PCF based sensor with high sensitivity, high birefringence and low confinement losses for liquid analyte sensing applications, Sensors 15 (12) (2015) 31833–31842.
[32] I.H. Malitson, Interspecimen comparison of the refractive index of fused silica, JOSA 55 (10) (1965) 1205–1209.
[33] S. Selleri, L. Vincetti, A. Cucinotta, M. Zoboli, Complex FEM modal solver of optical waveguides with PML boundary conditions, Opt. Quant. Electron. 33 (4–5) (2001) 359–371.
[34] B.Q. Wu, Y. Lu, C.J. Hao, L.C. Duan, N.N. Luan, Z.Q. Zhao, J.Q. Yao, Hollow-core photonic crystal fiber based on C_2H_2 and NH_3 gas sensor, Applied Mechanics and Materials, 411, 2013, pp. 1577–1580.
[35] N.A. Mortensen, Effective area of photonic crystal fibers, Opt. Express 10 (7) (2002) 341–348.
[36] G.P. Agrawal, Nonlinear fiber optics, Nonlinear Science at the Dawn of the 21st Century, Springer 2000, pp. 195–211.
[37] J. Broeng, D. Mogilevstev, S.E. Barkou, A. Bjarklev, Photonic crystal fibers: a new class of optical waveguides, Opt. Fiber Technol. 5 (3) (1999) 305–330.
[38] M.N. Petrovich, A. Van Brakel, F. Poletti, K. Mukasa, E. Austin, V. Finazzi, P. Petropoulos, E. O'Driscoll, M. Watson, T. DelMonte, et al., Microstructured fibers for sensing applications, Optics East 2005, 2005 (p. 60050E–60050E).
[39] H. Ebendorff-Heidepriem, P. Petropoulos, S. Asimakis, V. Finazzi, R. Moore, K. Frampton, F. Koizumi, D. Richardson, T. Monro, Bismuth glass holey fibers with high nonlinearity, Opt. Express 12 (21) (2004) 5082–5087.
[40] R.T. Bise, D.J. Trevor, Sol-gel derived microstructured fiber: fabrication and characterization, Optical Fiber Communications Conference (OFC), vol. 3, 2005.
[41] Y. Huang, Y. Xu, A. Yariv, Fabrication of functional microstructured optical fibers through a selective-filling technique, Appl. Phys. Lett. 85 (22) (2004) 5182–5184.
[42] M. Luo, Y. Liu, Z. Wang, T. Han, Z. Wu, J. Guo, W. Huang, Twin-resonance-coupling and high sensitivity sensing characteristics of a selectively fluid-filled microstructured optical fiber, Opt. Express 21 (25) (2013) 30911–30917.
[43] R.M. Gerosa, D.H. Spadoti, C.J. de Matos, L. de S. Menezes, M.A. Franco, Efficient and short-range light coupling to index-matched liquid-filled hole in a solid-core photonic crystal fiber, Opt. Express 19 (24) (2011) 24687–24698.
[44] F. Poletti, V. Finazzi, T.M. Monro, N.G. Broderick, V. Tse, D.J. Richardson, Inverse design and fabrication tolerances of ultra-flattened dispersion holey fibers, Opt. Express 13 (10) (2005) 3728–3736.